Report on projects associated to Contract No. 14402/00/NL/MV – CCN

Maria Grazia Pia
INFN Genova
MariaGrazia.Pia@ge.infn.it

23 July 2008

Abstract

This report summarizes the activities at INFN Genova associated to the appendix to Contract No. 14402/00/NL/MV. They concern the design and development of anthropomorphic phantom models based on Geant4, the validation of Geant4 low energy models for electron interactions and the investigation of extensions to model PIXE.

1 Anthropomorphic phantom

Realistic computational models of the human body are useful tools to study the effects of radiation through Monte Carlo simulation in various domains, such as radiation protection, oncological radiotherapy, radiology and nuclear medicine.

Several models of anthropomorphic phantoms have been developed in the past decades, representing a complete human body or parts of it. They are characterized by two different approaches to the description of body anatomy: the geometry of organs modelled either through mathematical equations or by means of digital volume arrays (voxels); in both types of phantoms a material composition is associated to each elementary geometrical component. The first anthropomorphic phantoms [1][2][3] were developed as analytical representations of relatively simple geometries; these models have been subsequently refined [4]. Voxel phantoms [5] are usually derived from computerized tomography or magnetic resonance images.

The issue of which modeling technique is superior has been debated at length in the scientific community: both mathematical and voxel phantoms present advantages and drawbacks [6]. In a pragmatic view they are both valuable, as their different characteristics are suitable to address different application requirements. Similarly, the availability of a variety of models even within the same category of phantoms offers a wide choice of features relevant to different contexts of usage.

Software implementations of phantom models have been developed based on both approaches; in most cases, however, the software is not publicly available to the scientific community. In this perspective an open source software system providing a variety of anthropomorphic phantom models in the same simulation setting would be a useful contribution to the scientific community.

The Geant4 [7][8] toolkit offers a particularly suitable environment for the development of such tool: the object oriented technology, on which it is based, facilitates the provision of alternative models, while the full-fledged functionality of Geant4 geometry and material packages well supports the implementation of anthropomorphic phantom models. Other Geant4 features, like methods for efficient navigation across volumes and sophisticated techniques for memory optimization in large scale geometries, are relevant to the effective usage of anthropomorphic phantoms in a simulation. The Human Phantom project described here provides phantom models based on Geant4.

The first development cycle, which is described here, devised a novel approach to anthropomorphic phantoms based on modern software technology and focussed on creating an environment for multiple phantom models. The software system created is characterized by an original design, which enables the development of different phantom modelling approaches and their transparent usage in simulation applications, irrespective of their specific technical features or implementation details.

A first version of the software has been publicly released with Geant4 as part of the Advanced Examples package.

1.1 Analysis and design

The object oriented analysis identified two main abstractions: the process of assembling a phantom and its underlying model of the human body. These two concepts characterize the architecture of the package.

An anthropomorphic phantom can be considered as the result of assembling the various anatomical components of the human body according to a defined sequence. The process of building a phantom is handled through a Builder design pattern [9]: this pattern allows the separation of the construction process of a complex object, such as an anthropomorphic phantom, from its representation; therefore, the same construction process can create different representations. The related class diagram, expressed through the Unified Modeling Language (UML) [10], is illustrated in Figure 1.

The *GHPBasePhantomBuilder* base class defines the interface for assembling a phantom. It establishes a set of member functions responsible for constructing individual components of the phantom, and a *GetPhantom* member function to retrieve the result of the assembly process, that is the complete phantom constructed, as an object of *GHPVPhysicalVolume* type compatible with Geant4 geometry. *GHPBasePhantomBuilder* is a concrete class, which provides dummy implementations of all its public virtual member functions: its responsibility consists of defining the building process only. Subclasses of *GHPBasePhantomBuilder* provide actual implementations of the assembly process.

The derived classes have the opportunity to select which virtual member functions to implement: therefore, they can specialize the assembly process by building the subset of anatomical components specific to a given sex, or adequate to the requirements of a given application, or corresponding to partial models Any subclasses of *GHPBasePhantomBuilder* can be handled polymorphically in a user application through the same base class interface: therefore, the same building process defined can result in different phantom representations transparently.

The Geant4 Human Phantom package provides a *GHPPhantomBuilder* derived class and two further specializations of it, *GHPFemalePhantomBuilder* and *GHPMalePhantomBuilder*. *GHPPhantomBuilder* is responsible for assembling the body parts common to both sexes by overloading the corresponding member functions of its base class; *GHPFemalePhantomBuilder* and *GHPMalePhantomBuilder* overload the member functions of *GHPBasePhantomBuilder* modelling the organs specific to each sex.

Alternative assembly processes can be easily customized by deriving classes from *GHPBasePhantomBuilder* and overloading the desired member functions. For instance, if a partial body representation is adequate to satisfy the application requirements, the design allows the user to assemble a customized phantom consisting of the desired body components only: it would be sufficient to provide concrete implementations of the virtual functions corresponding to the anatomical components of interest in the derived class, while the dummy implementations of the base class would be retained for the other steps of the assembly process.

The building process allows the user to specify the sensitivity of each body component to be constructed, that is its capability to record the dose deposited in it. It also provides other options useful in a typical simulation application, like the ability to determine the location where the constructed phantom is positioned and parameters for its graphical representation.

The phantom building process is independent from the features of phantom model to be constructed: this sharp domain decomposition is a key feature of the software design, and determines the generality and the flexibility of the software system developed.

The creation of coherent models of the human body is handled through an Abstract Factory design pattern [9]. A *GHPVBodyFactory* abstract base class defines the interface for creating anatomy components; concrete factories derived from it implement the actual creation of body parts. Each factory is responsible for creating a family of products corresponding to a phantom model: either one of the established phantoms documented in literature or a user-defined one. The products created are of *G4VPhysicalVolume* type: this is the abstract class of the Geant4 Geometry package defining the

interface of physical volumes. The class diagram illustrating the creation of coherent phantom models is shown in Figure 2.

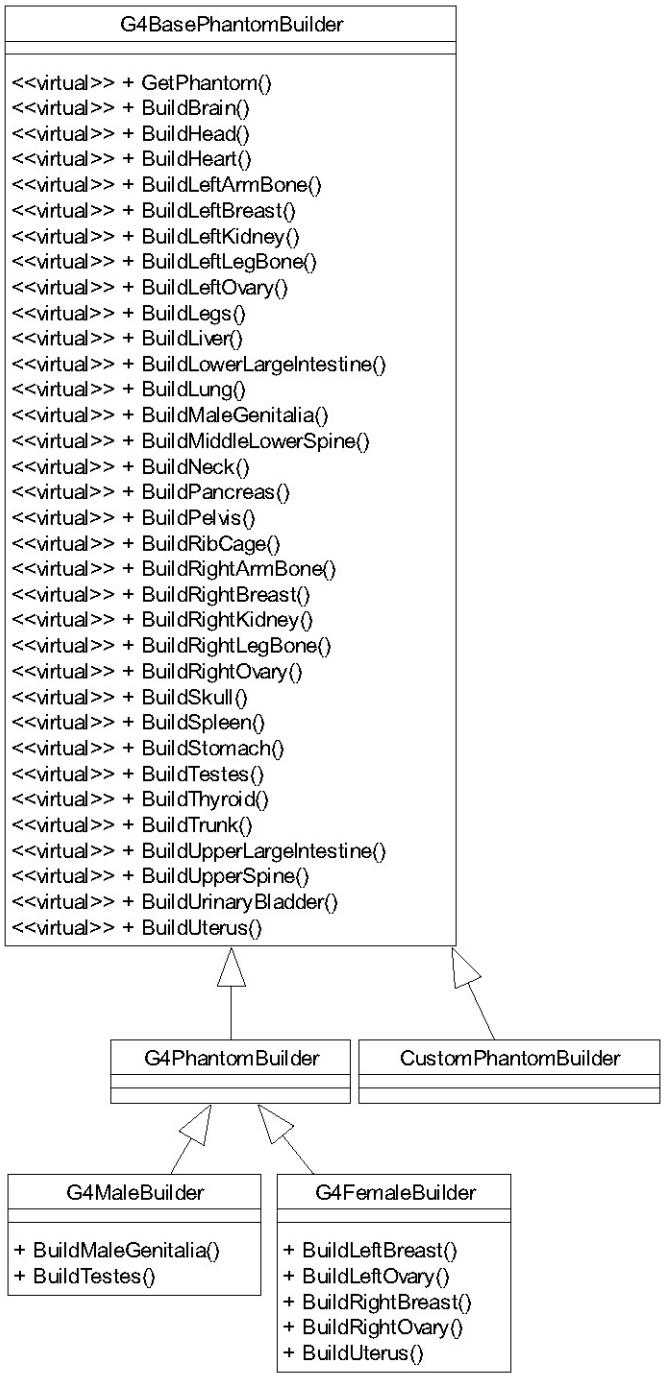

Figure 1 The UML class diagram shows the main design features of the phantom construction process.

A phantom builder may be associated to one or more body factories, thus enabling the assembly of standard phantom models, or of combinations of their parts, as well as user-defined body models. For instance, in the design model of Figure 2 a phantom builder aggregates a body factory object as one of its attributes; this object is associated to the phantom builder as an argument of its constructor. The phantom builder delegates the actual construction of the body components to its associated factory: each of member function responsible to build a specific body part sends a message to the associated factory to create it.

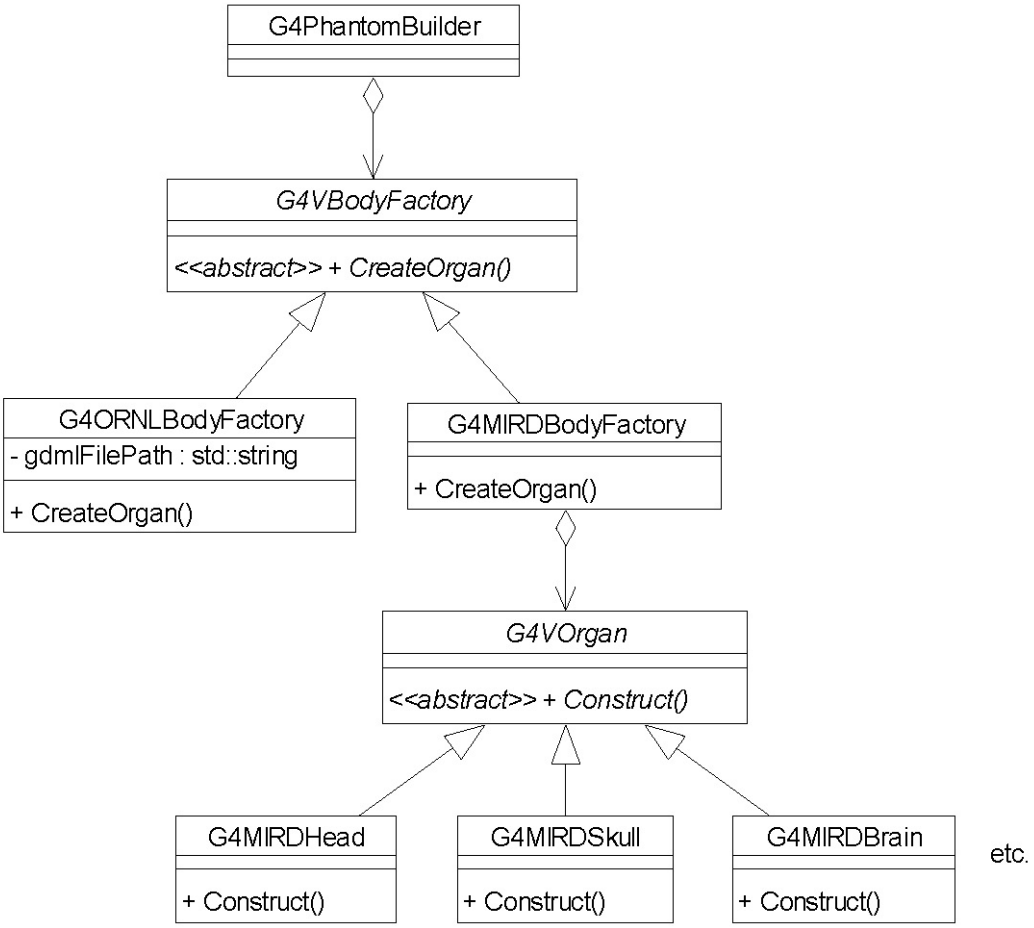

Figure 2 The UML class diagram illustrates the main design features of the creation of human body models and their association to the phantom construction.

1.2 Implementation of phantoms

The design of the Geant4 Human Phantom package is open to a variety of implementations of phantom models. Two established analytical ones, the MIRD [2] and the ORNL [3] phantoms, are implemented in the first released version of the package: they provide Geant4 users the functionality of these two concrete models, but they also represent different examples of implementation approaches useful as guidance for further extensions of the package.

A solution of general applicability has been developed to facilitate the implementation of phantom models. Its conceptual approach consists of separating the data describing an anthropomorphic phantom from their usage in the software; the persistency scheme adopted is independent from any specific characteristics of the phantoms. It is worthwhile stressing that by data one does not mean numerical parameters only, but more in general the information content essential to model anatomical components as geometrical entities.

The solution developed exploits the Geometry Description Markup Language (GDML) [11], an open source software tool suitable to describe complex geometry models. In this approach the actual geometry and material description of a phantom is delegated to a GDML specification, while a body factory implementation only retains the responsibility of accessing it and of instantiating the corresponding Geant4 physical volume objects.

The GDML description of a phantom consists of a collection of independent, standalone files, each one associated to a body component. The description is based on the concept of the geometry tree, which is defined by specifying the mother-daughter relations between different volumes. Any volume can contain other volumes inside, positioned and rotated with respect to the local (mother's) coordinate system. Each volume is represented by the associated solid and is composed of a specific material.

The phantom geometry is then instantiated in memory by combining several GDML files corresponding to the desired anatomy components. The fine granularity of the representation enables a flexible configuration of the final product. This scheme makes it possible to run different phantom configurations (using, for instance, different descriptions of some parts of the body) without the need to change the actual geometry construction implementation in the user simulation code.

This implementation solution provides great versatility to describe different phantom models and flexibility to customize them. In this context, the creation of different phantom models is reduced to the specification of the data of their components in GDML files, without requiring any additional coding. This scheme also leads to a convenient customization of body descriptions: for instance, one may easily change the size, position and material composition of an organ, or even its shape, by modifying the corresponding GDML file, without needing any modification of the simulation code nor its recompilation. The realization of a female anthropomorphic phantom is shown in Figure 3.

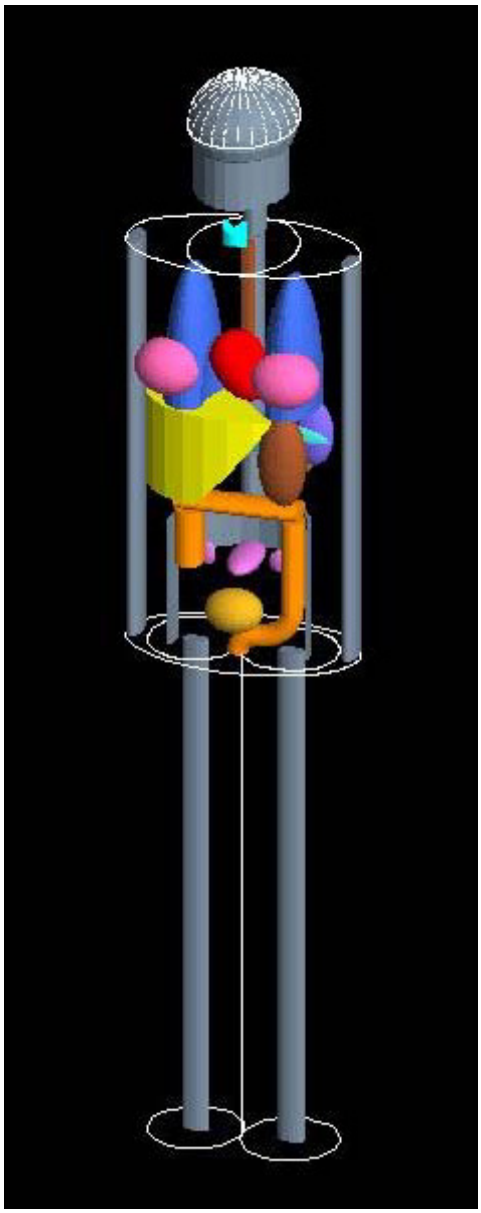

Figure 3 Example of a human phantom.

The MIRD phantom model is handled by an associated concrete factory, *GHPMIRDBodyFactory*. The implementation of this factory exploits a set of individual classes, each one responsible for the model of a single body component according to the original MIRD model. The granular design of this model facilitates the reuse of individual MIRD phantom components in user-defined phantom models, for instance mixing some MIRD components with other descriptions of body elements. The MIRD phantom represents a hermaphrodite human body.

The ORNL phantoms consist of a set of body descriptions respectively for an adult female, an adult male and children of different ages. Their implementation exploits the scheme based on GDML.

All the ORNL phantoms are handled by one factory, *GHPGDMLBodyFactory*; a collection of GDML files provide specialized phantom descriptions for different ages and sex. Each ORNL phantom is organized as collection of GDML files in an associated directory of the file system; *GHPGDMLBodyFactory* holds the directory name as one of its attributes; its value is supplied through one of the arguments of the class constructor: therefore, the user can instantiate the factory object corresponding to the phantom specialization of her or his choice.

To demonstrate the capabilities of the design developed, a female phantom embedding a voxel breast in an analytical body representation has been implemented. The voxel breast is based on the model described in [12]; it is implemented in the *GHPCompressedVoxelBreast* class. The *GHPCustomizedPhantomBuilder* is responsible of the process of building the phantom; it overrides the *BuildLeftBreast* member function of *GHPBasePhantomBuilder* by implementing the creation of a voxel breast as described above, while all the other anatomical components are built exploiting the *GHPGDMLBodyFactory* and the set of GDML files pertinent to an ORNL female phantom. Figure 4 shows the resulting mixed phantom.

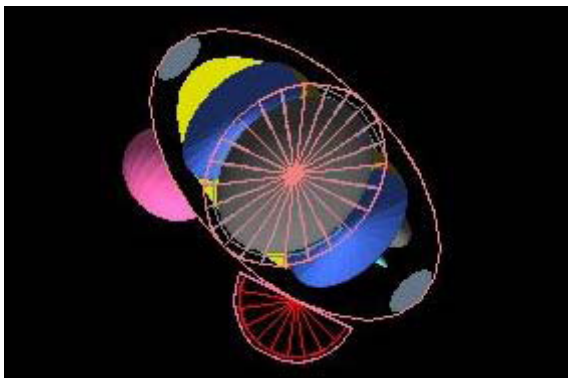

Figure 4 Example of a mixed analytical and voxel phantom: the right and left breasts are based on either type of representation.

2 Validation of low energy electron models

The high precision experimental data in [13] have represented a prime reference for benchmarking all major Monte Carlo codes in the low energy range up to approximately 1 MeV. The experiment was indeed set-up specifically for the validation of the ITS [13] Monte Carlo system.

Preliminary and partial comparisons, like [15] and [16], have been performed against these data with previous Geant4 versions; however, a thorough study of Geant4 low energy electron-photon interaction models in relation to the full experimental data set has not been published yet to complement the comparisons against the NIST physical reference data [17]. Therefore, this project was focussed on producing a systematic assessment of Geant4 electron-photon models in the low energy electromagnetic package [17][19] against this authoritative reference.

Moreover, since Geant4 multiple scattering algorithm, i.e. one of the most critical elements of a Monte Carlo transport system, has recently undergone significant evolution, this study also investigated the effects of such changes in a real-life experimental set-up involving low energy interactions. For this purpose the tests reported here were performed with multiple Geant4 versions

corresponding to different implementations of the multiple scattering, while all the other electron-photon physics models involved in the simulation remained unchanged.

2.1 Experimental set-up

The data sets cover different target materials, spanning a wide range in atomic number from beryllium to uranium.

Calorimetric measurement techniques were applied to determine the physical observables under investigation. A calorimeter foil was placed between a front layer and a "semi-infinite" backward layer (i.e. a slab thicker than the range of most electrons) to measure the energy deposition at a specified distance from the target surface. The calorimeter was made of the same material as the entire target configuration.

For a given front slab, the measurement depth was determined as the slab thickness plus half the calorimeter thickness. Measurements were performed for different thicknesses of the front layers.

The uncertainty in the experimental energy deposit is less than 2.2%.

2.2 Simulation set-up

The energy spectrum of primary electrons was modelled as a Gaussian curve, where the standard deviation was taken to be the error associated with the measurement of the beam energy specified in [13].

The target consisted of a cylinder and was defined as a sensitive detector; the energy deposition was scored in slabs placed inside the target.

It is worthwhile stressing that the geometrical description of the simulation set-up corresponded exactly to the experimental one: for instance, this requirement implied that the simulations were performed as multiple single runs, each of them reproducing the accurate calorimeter positioning as documented in the experimental reference, rather than scoring the energy deposit in regular slices of the target material. The accurate reproduction of the experimental condition was verified to make a difference in the simulation results.

The physics processes activated in the simulations were the library-based [20][21][22] and the Penelope-like [23] models contained in the Geant4 Low-Energy package and the multiple-scattering model of the Standard package.

The secondary production threshold was set to be the minimum value recommended for use with Geant4 low energy package, i.e. the equivalent of 250 eV in range in all the materials considered. The maximum step size was set to a value comparable with the thickness of the scoring slabs. The considered experimental bin sizes were 0.001 mm for lower beam energies and 0.015 mm for beams of 1 MeV; thus the maximum step size was set to 0.001 mm for all simulation runs.

2.3 Results

The comparison concerned the experimental data sets in [13] consisting of homogeneous media. The results concerning normally incident beams are reported here only; those corresponding to 60 degrees incidence are similar.

The results show good agreement of Geant4 low energy models with the experimental data, except for uranium. Geant4 low energy models based on the Livermore libraries appear to be in general as accurate as, or more accurate than the Penelope-like ones, with the exception of the tests concerning uranium. A systematic effect, either in the experimental data or in the theoretical calculations underlying the evaluated data libraries, is suspected to occur in this material set-up.

The accuracy of the results with Geant4 9.1 appears in general as good as, or better than the one with Geant4 8.1p02; this outcome demonstrates on an experimental ground that the evolution of the multiple scattering algorithm improved the simulation accuracy at low energies. It is worth remarking that the study reported in [16] was performed with Geant4 version 8.1.

2.3.1 Berillium (Z=4)

The results are reported in the following figures for incident electron energies of 58 keV, 109 keV, 314 keV, 521 keV and 1.033 MeV.

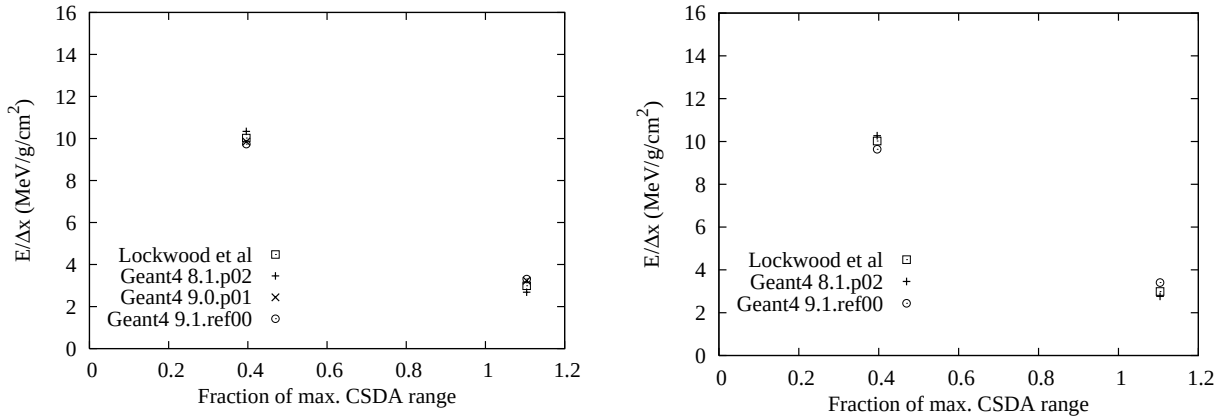

Figure 5 Energy deposit as a function of fraction of the CSDA range: Geant4 library-based (left) and Penelope-like (right) low energy models, Be target, 58 keV incident electrons.

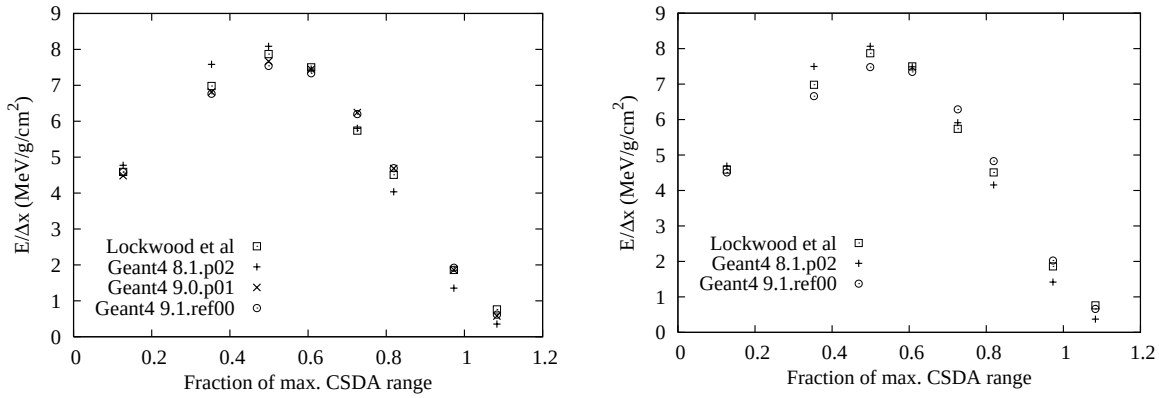

Figure 6 Energy deposit as a function of fraction of the CSDA range: Geant4 library-based (left) and Penelope-like (right) low energy models, Be target, 109 keV incident electrons.

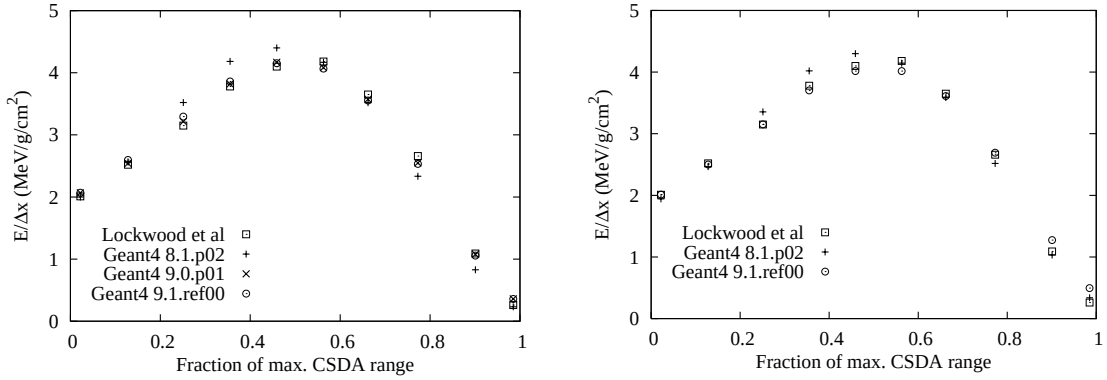

Figure 7 Energy deposit as a function of fraction of the CSDA range: Geant4 library-based (left) and Penelope-like (right) low energy models, Be target, 314 keV incident electrons.

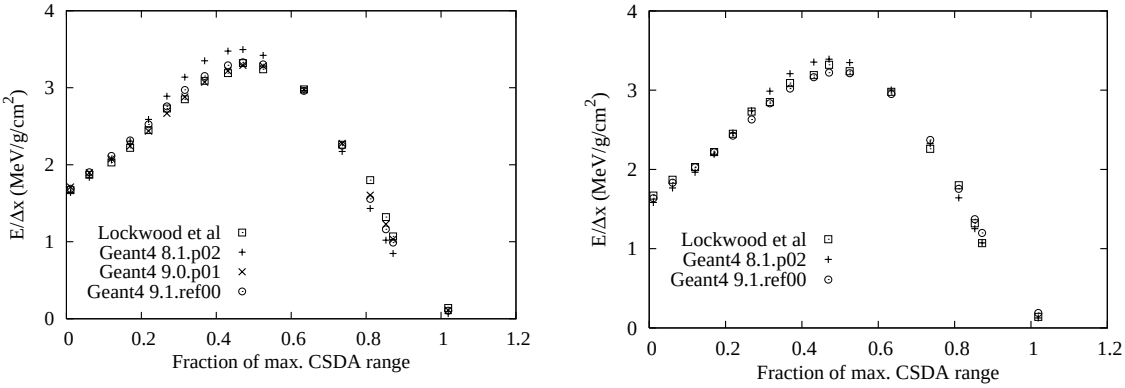

Figure 8 Energy deposit as a function of fraction of the CSDA range: Geant4 library-based (left) and Penelope-like (right) low energy models, Be target, 521 keV incident electrons.

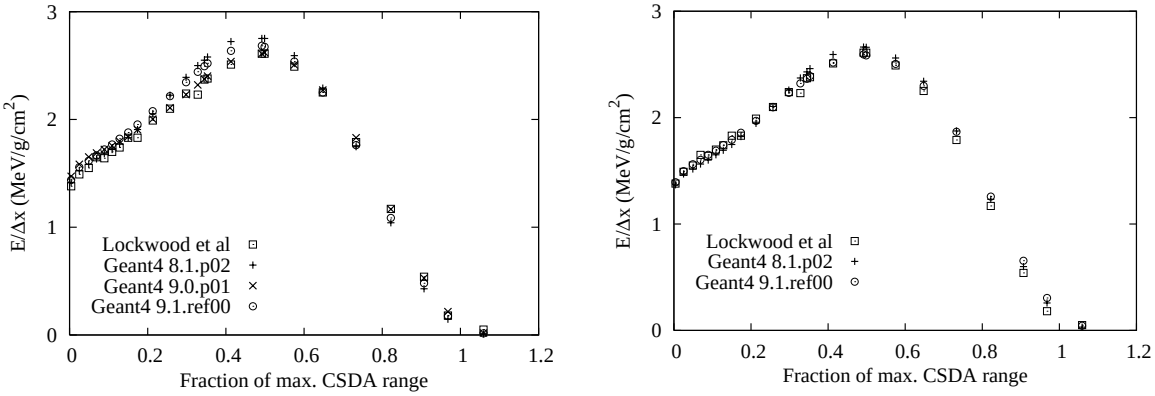

Figure 9 Energy deposit as a function of fraction of the CSDA range: Geant4 library-based (left) and Penelope-like (right) low energy models, Be target, 1033 keV incident electrons.

2.3.2 Aluminium (Z=13)

The results are reported in the following figures for incident electron energies of 314 keV, 521 keV and 1.033 MeV.

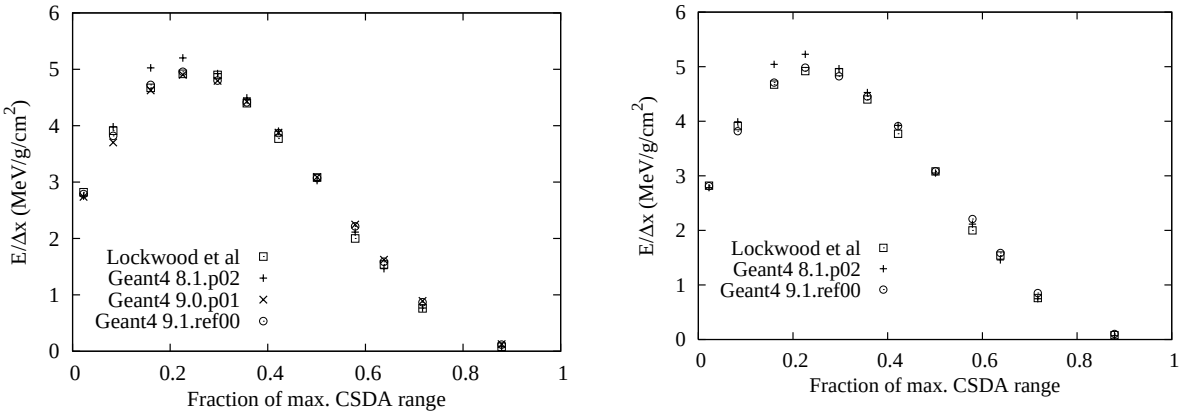

Figure 10 Energy deposit as a function of fraction of the CSDA range: Geant4 library-based (left) and Penelope-like (right) low energy models, Al target, 314 keV incident electrons.

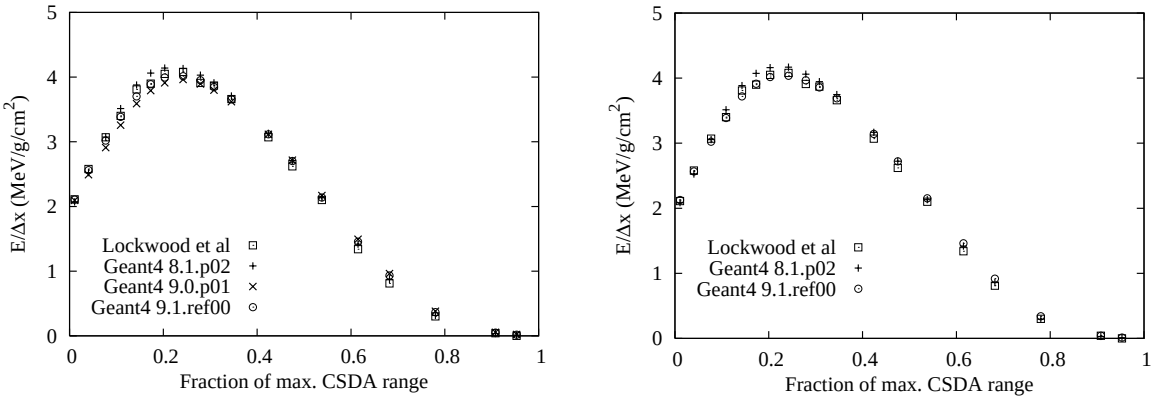

Figure 11 Energy deposit as a function of fraction of the CSDA range: Geant4 library-based (left) and Penelope-like (right) low energy models, Al target, 521 keV incident electrons.

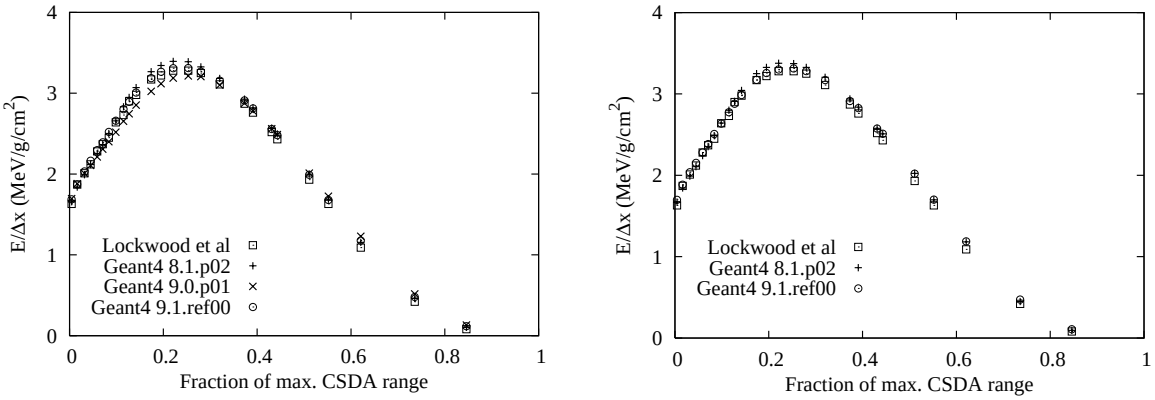

Figure 12 Energy deposit as a function of fraction of the CSDA range: Geant4 library-based (left) and Penelope-like (right) low energy models, Al target, 1033 keV incident electrons.

2.3.3 Iron (Z=26)

The results are reported in the following figures for incident electron energies of 300 keV, 500 keV and 1 MeV.

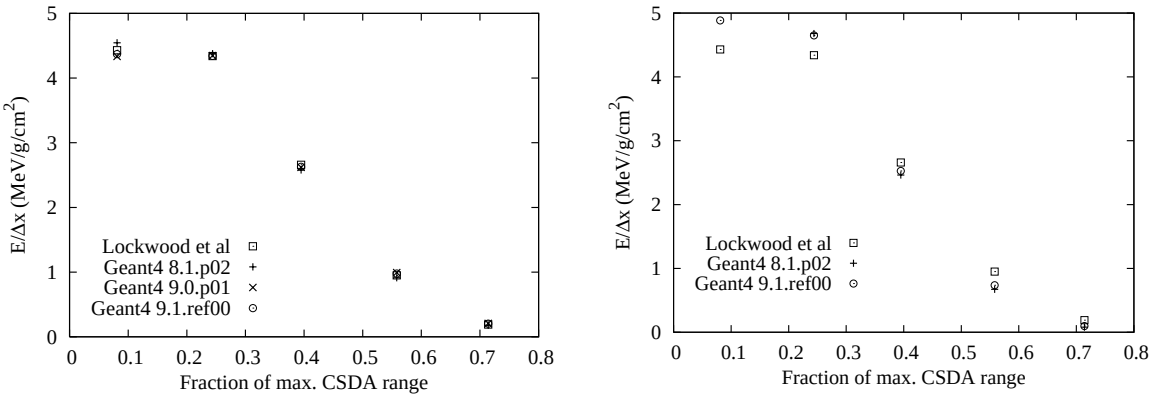

Figure 13 Energy deposit as a function of fraction of the CSDA range: Geant4 library-based (left) and Penelope-like (right) low energy models, Fe target, 300 keV incident electrons.

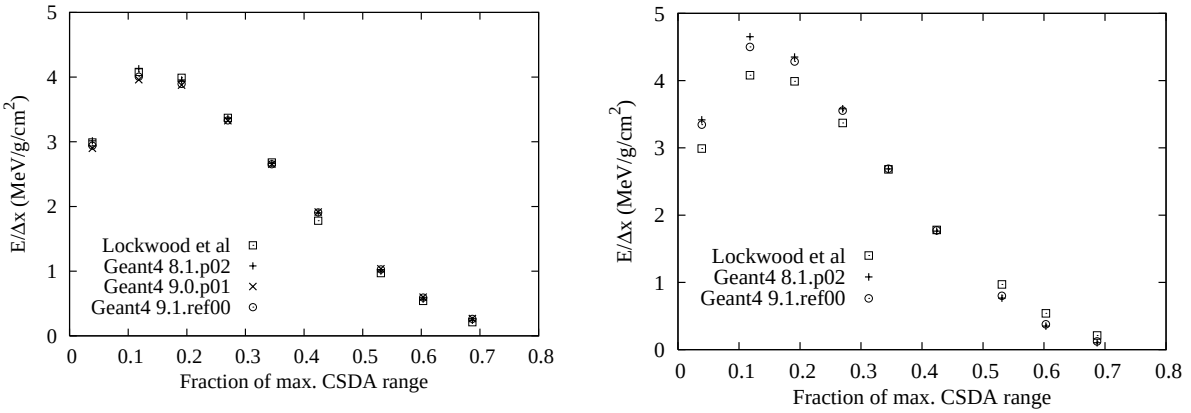

Figure 14 Energy deposit as a function of fraction of the CSDA range: Geant4 library-based (left) and Penelope-like (right) low energy models, Fe target, 500 keV incident electrons.

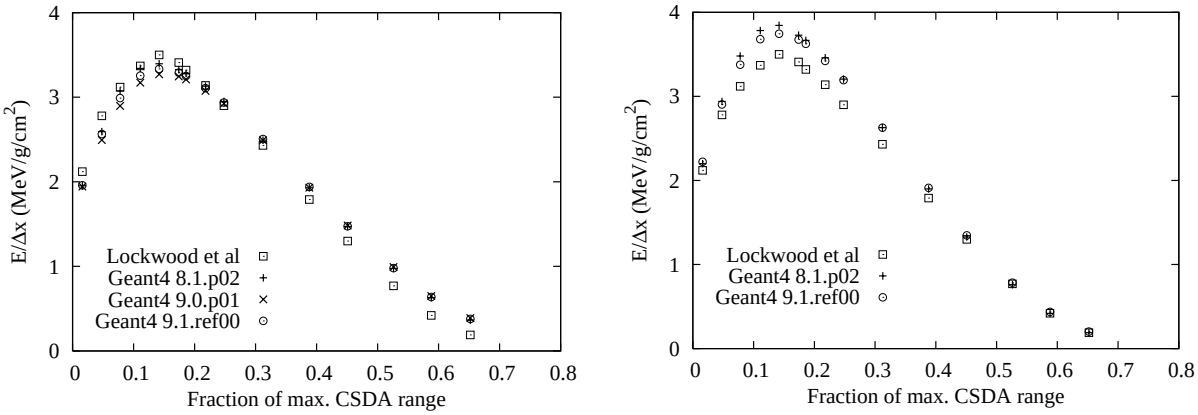

Figure 15 Energy deposit as a function of fraction of the CSDA range: Geant4 library-based (left) and Penelope-like (right) low energy models, Fe target, 1 MeV incident electrons.

2.3.4 Copper (Z=29)

The results are reported in the following figures for incident electron energies of 300 keV and 500 keV.

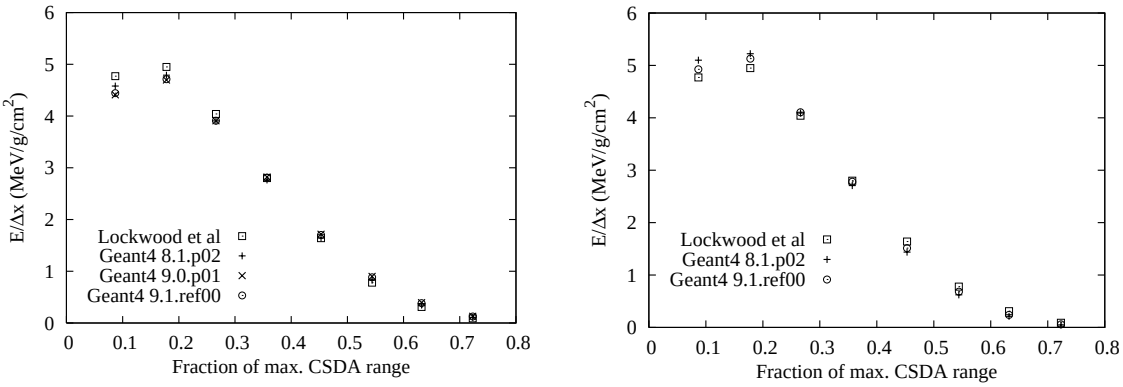

Figure 16 Energy deposit as a function of fraction of the CSDA range: Geant4 library-based (left) and Penelope-like (right) low energy models, Cu target, 314 keV incident electrons.

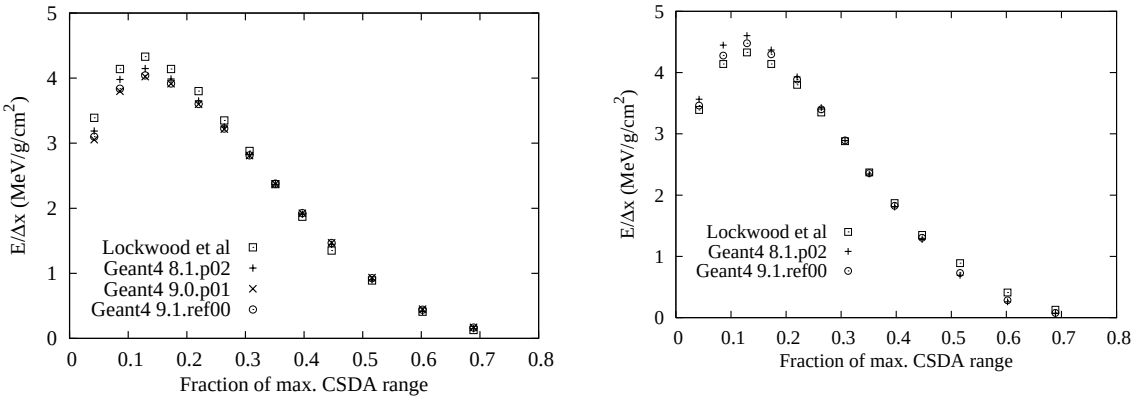

Figure 17 Energy deposit as a function of fraction of the CSDA range: Geant4 library-based (left) and Penelope-like (right) low energy models, Cu target, 500 keV incident electrons.

2.3.5 Molybdenum (Z=42)

The results are reported in the following figures for incident electron energies of 100 keV, 300 keV, 500 keV and 1 MeV.

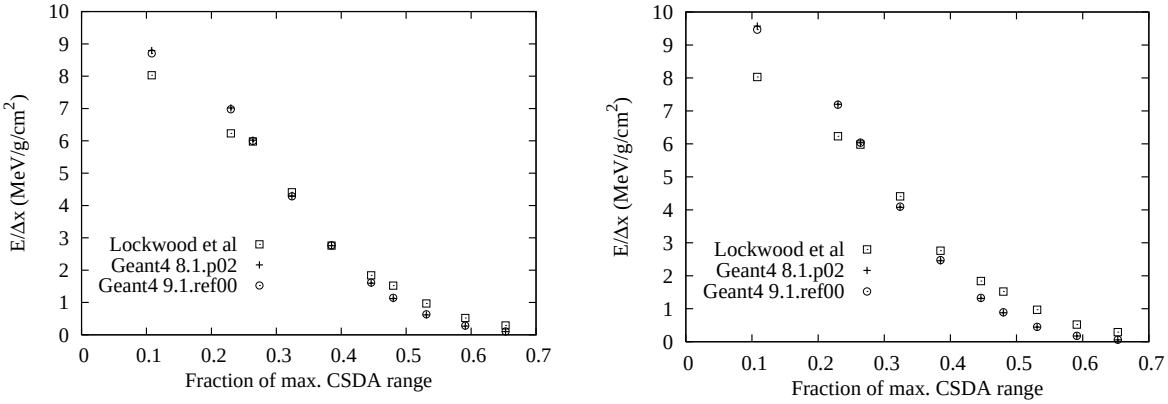

Figure 18 Energy deposit as a function of fraction of the CSDA range: Geant4 library-based (left) and Penelope-like (right) low energy models, Mo target, 100 keV incident electrons.

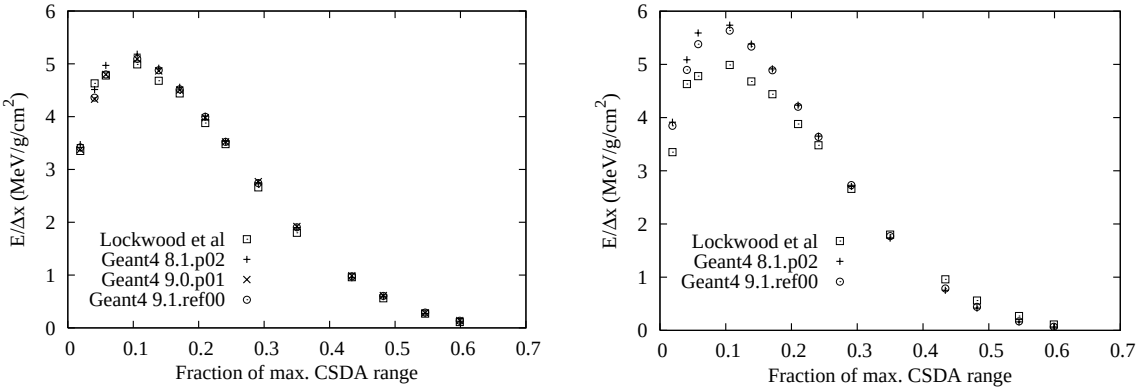

Figure 19 Energy deposit as a function of fraction of the CSDA range: Geant4 library-based (left) and Penelope-like (right) low energy models, Mo target, 300 keV incident electrons.

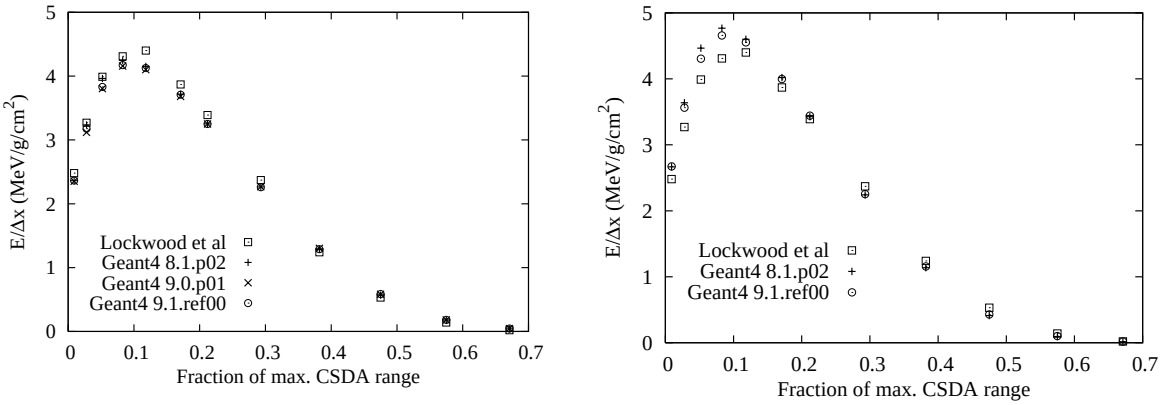

Figure 20 Energy deposit as a function of fraction of the CSDA range: Geant4 library-based (left) and Penelope-like (right) low energy models, Mo target, 500 keV incident electrons.

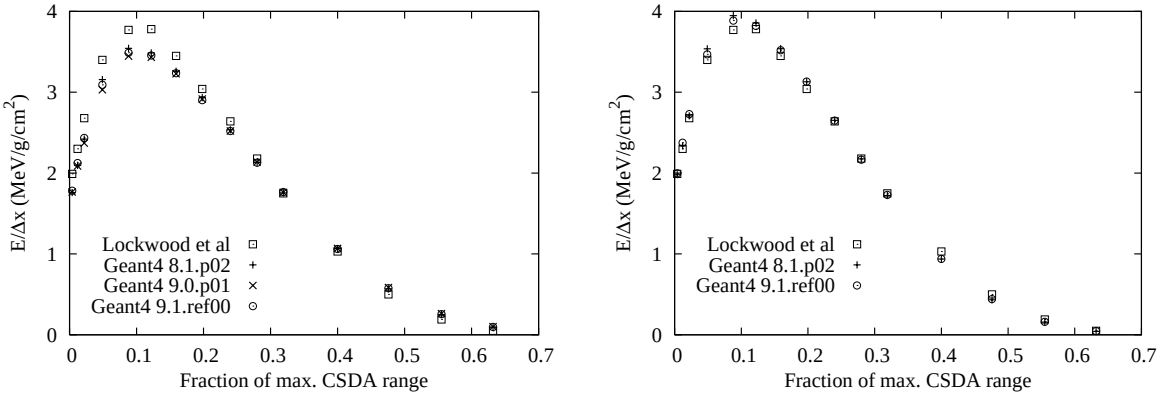

Figure 21 Energy deposit as a function of fraction of the CSDA range: Geant4 library-based (left) and Penelope-like (right) low energy models, Mo target, 1 MeV incident electrons.

2.3.6 Tantalum (Z=73)

The results are reported in the following figures Figure 9for incident electron energies of 300 keV, 500 keV and 1 MeV.

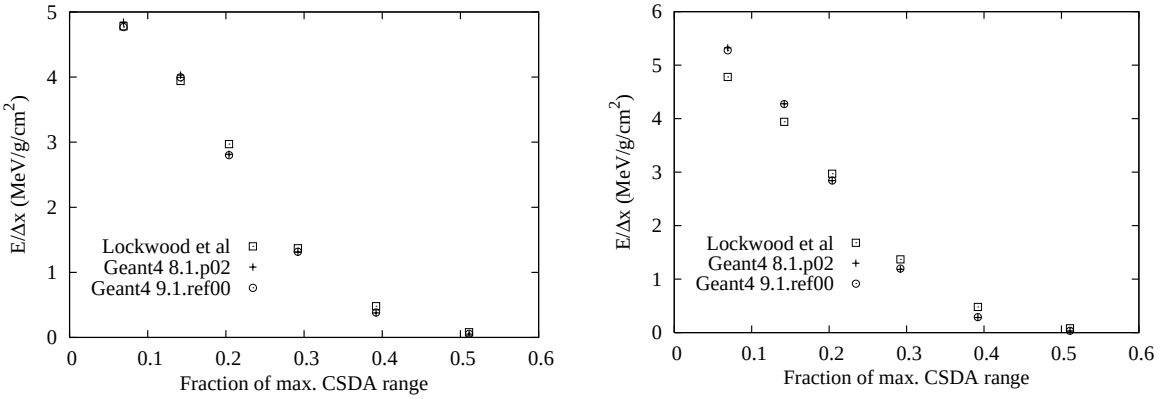

Figure 22 Energy deposit as a function of fraction of the CSDA range: Geant4 library-based (left) and Penelope-like (right) low energy models, Ta target, 300 keV incident electrons.

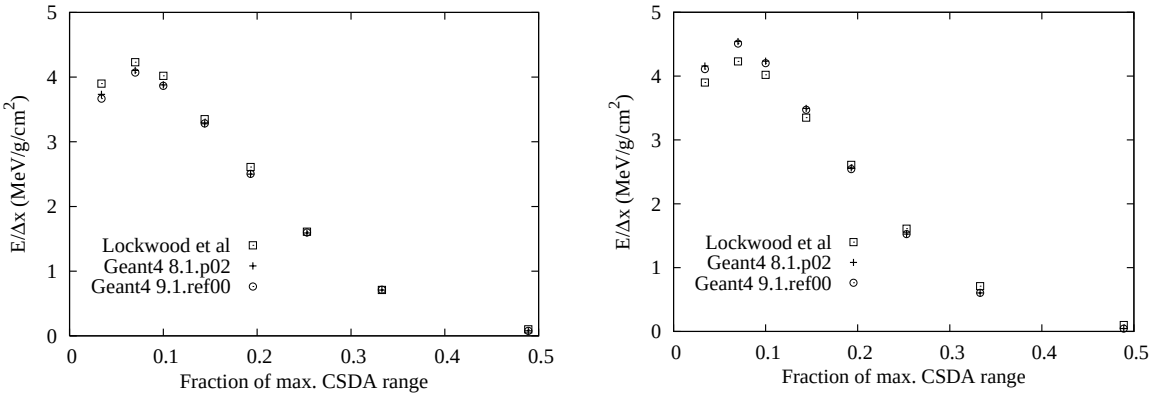

Figure 23 Energy deposit as a function of fraction of the CSDA range: Geant4 library-based (left) and Penelope-like (right) low energy models, Ta target, 500 keV incident electrons.

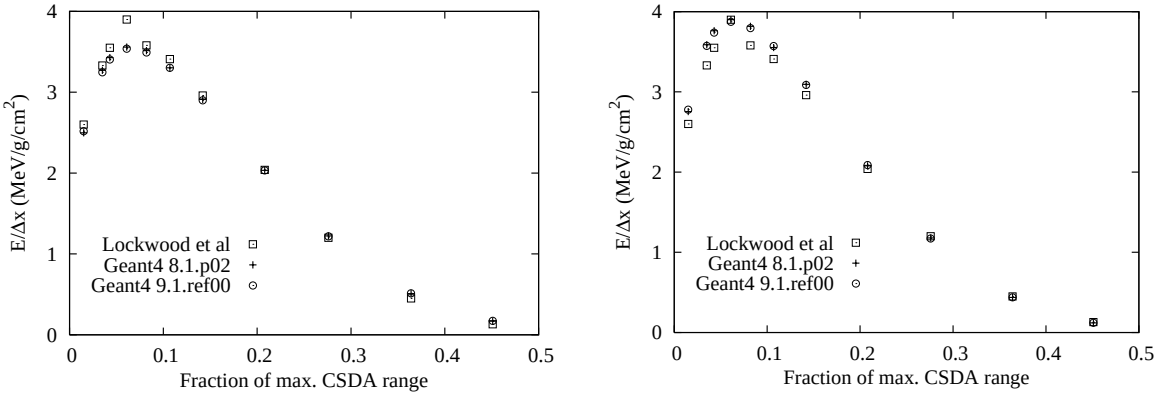

Figure 24 Energy deposit as a function of fraction of the CSDA range: Geant4 library-based (left) and Penelope-like (right) low energy models, Ta target, 1 MeV incident electrons.

2.3.7 Uranium (Z=92)

The results are reported in the following figures Figure 9for incident electron energies of 300 keV, 500 keV and 1 MeV.

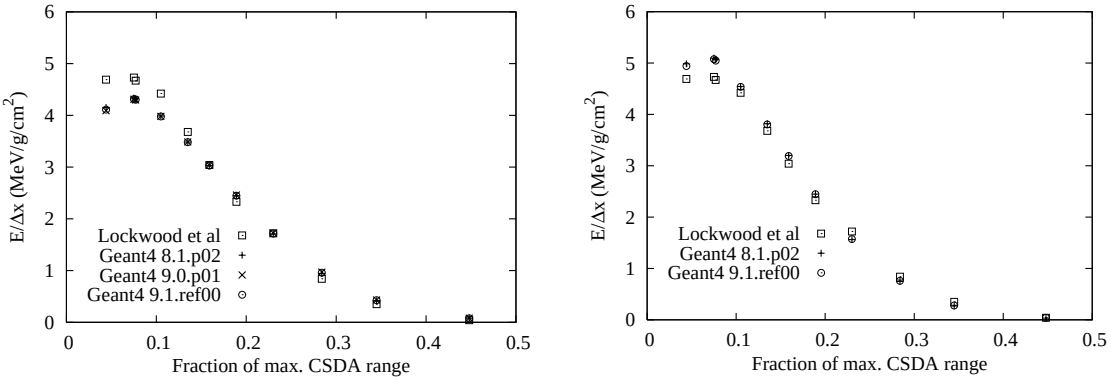

Figure 25 Energy deposit as a function of fraction of the CSDA range: Geant4 library-based (left) and Penelope-like (right) low energy models, U target, 300 keV incident electrons.

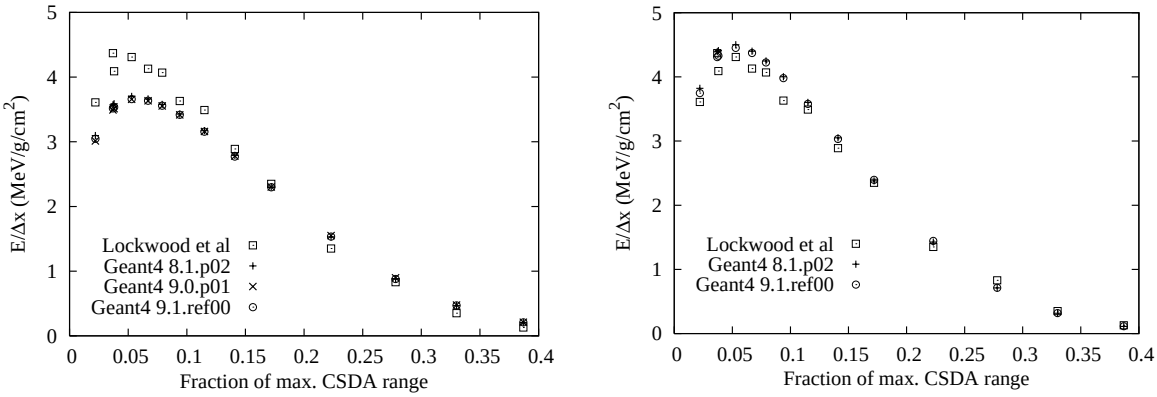

Figure 26 Energy deposit as a function of fraction of the CSDA range: Geant4 library-based (left) and Penelope-like (right) low energy models, U target, 500 keV incident electrons.

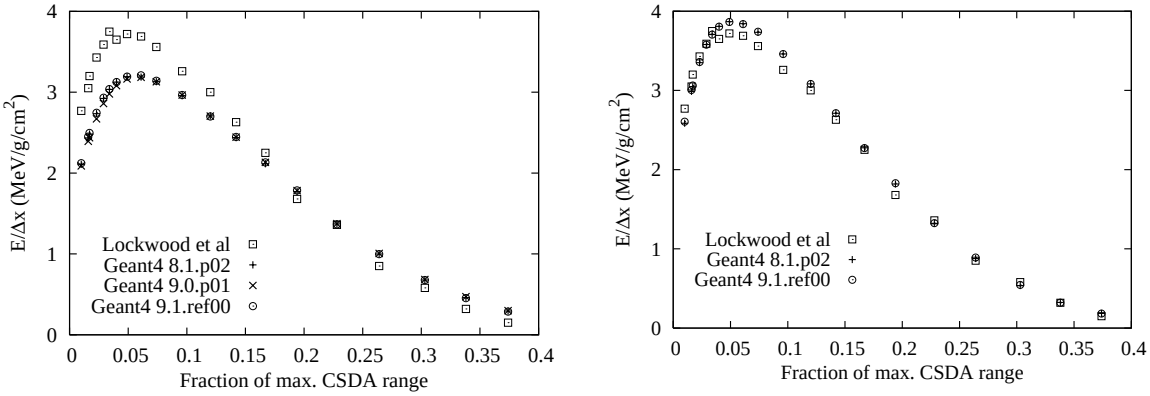

Figure 27 Energy deposit as a function of fraction of the CSDA range: Geant4 library-based (left) and Penelope-like (right) low energy models, U target, 1 MeV incident electrons.

3 PIXE simulation

The simulation of PIXE (Particle Induced X-ray Emission) is of interest to various experimental applications involving material analysis in diverse fields like geology, planetary astrophysics, environmental sciences, archaeology and fine arts. The process of atomic relaxation can also influence accurate dosimetry. The X-rays resulting from PIXE may also contribute to the non-physical background of science-driven space missions.

Geant4 low energy electromagnetic package includes a model of K-shell vacancy creation cross sections for incident proton ionization, based on fits to a systematic collection of experimental data in [24]. Further extensions of Geant4 PIXE simulation capabilities have been investigated in this project.

3.1 Problem domain analysis and prototype implementation

The simulation of PIXE in Geant4 is reduced to the problem of identifying the shell where a vacancy is produced as a result of the ionization of the target atom due to the impact of a charged hadron or ion: in fact, once the vacancy in the shell occupation occurs, the Geant4 Atomic Relaxation [25] package takes charge of generating the secondary fluorescence X-rays and Auger electrons resulting from the de-excitation of the atom.

A design has been developed in the course of the first Geant4 PIXE development to treat polymorhically a variety of models to calculate ionization cross sections for different shells. Therefore, this project focussed on the analysis of the existing theoretical and experimental literature to identify the state of the art in the calculation of ionization cross sections for different incident particles, atomic shells and primary particle energies.

The ECPSSR [26] model is supported by a wide consensus in the scientific community. Therefore, this approach can be adopted for modelling ionization cross sections in Geant4 due to incident protons, α particles and ions. Further refinements, like the incorporation of corrections for the relativistic Dirac-Hartree-Slater nature of the K-shell [27], are documented in literature.

In principle the cross section calculations based on ECPSSR can be extended from low energies (of the order of 1 keV or even less) up to very high energies (or the order of 1 GeV); nevertheless, the accuracy of the theoretical approach degrades on both ends. A method to improve the simulation accuracy at high energies is currently under investigation; however, theoretical calculations requiring appropriate expertise are needed to obtain practical results suitable for implementation in Monte Carlo software. Contacts with theorists are in progress to ensure their essential collaboration for this purpose.

The implementation in Geant4 of the ECPSSR cross section model and its variants of corrections and refinements is based on the creation of an original data library derived from theoretical calculations. This approach is particularly suitable to Monte Carlo applications, as demonstrated by the exploitation of the Livermore Libraries for Geant4 electron-photon processes; it also provides great versatility to evaluate different modelling options and to extend the software capabilities to new developments, which are all treated transparently through interchangeable data files. Multiple data sets are being created for each element, corresponding to different theoretical calculations: plain ECPSSR, ECPSSR with corrections, first Born approximation [28] etc. This approach also allows the exploitation of experimental data collections as the basis of empirical models: in fact, a model based on [24] has been developed at INFN Genova. The creation of the Geant4 PIXE Data Library is in progress at INFN Genova.

In terms of software, the physics data management package developed at INFN Genova to handle the Geant4 models based on the Livermore Libraries can be exploited for modelling the cross sections involved in PIXE. This software is capable of data file management, data interpolation with a variety of algorithms, random number generation according to given interaction probabilities etc. The results presented in the following pages have been produced with a prototype implementation based on this software approach. Once more, the reusability of this software demonstrates that its sound object oriented design was a worthwhile investment.

Nevertheless, it should not be forgotten that the simulation of PIXE in Geant4 would be affected by conceptual limitations due to Geant4 treatment of ionization intrinsic to a condensed-random-walk scheme. In this approach, Geant4 (like all other major Monte Carlo codes) handles the infrared divergence affecting the ionization process through a continuous energy loss component and a discrete one; this treatment affects the generation of PIXE, which is intrinsically a discrete process. A collaboration is in progress between INFN Genova and an experimental group at MPI to evaluate the extent of this limitation in realistic applications; nevertheless a conceptually correct simulation of PIXE requires a deep revision of the whole ionization design. Given the complexity of the issues involved, a dedicated R&D is foreseen in this domain.

3.2 Sample results

The following figures illustrate a sample of results concerning the ionization cross section models developed for the simulation of PIXE with Geant4. The results are shown for the ionization of Au (Z=79) by incident protons and concern calculations based on the ECPSSR models and on the first Born approximation; they demonstrate the capability of calculating cross sections for the creation of vacancies in K, L and M shell to the detail of individual sub-shells. Figure 28 shows the relative importance of cross sections for the ionization of K, L and M shells: several orders of magnitude are concerned.

Experimental data from [24] for K-shells and [29] for L-shells are superimposed to the calculated cross sections: in the case of [24] they derive from an evaluation process of measurements documented in literature, while [29] reports individual measurements, which in some cases exhibit evident discrepancies among the experiments. The plots demonstrates a relatively good agreement between the ECPSSR model and experimental data; at higher energies the plane wave Born approximation and the ECPSSR model behave similarly, while at lower energies the improvement brought by the ECPSSR treatment is evident. Variants of the ECPSSR model further improve the

agreement in the intermediate energy range considered, while in some cases they appear to slightly worsen the accuracy in the lower and higher energy ends. A systematic study of the range of applicability of various corrections documented in literature is in progress; due to the various elements involved (types of theoretical corrections, energy range, atomic number range, systematic errors of the reference experimental data) a thorough assessment of the applicability of such corrections as effective improvements to the model requires a significant investment of time and effort.

Hardly any experimental data are available for M-shells; the few documented in literature fold in ionization cross sections with X-ray production ones, thus preventing a direct validation of the theoretical ionization cross section model. Sparse experimental measurements are available at energies above 10 MeV: in fact, the range of PIXE application for material analysis involves energies around a few MeV.

3.3 Further developments in progress

The preliminary results indicate that the modelling approach devised for the calculation of shell ionization cross sections by hadrons and ions is a suitable basis for the simulation of PIXE. Therefore the production of a data library for the whole periodic system is in progress, concerning incident protons, α particles and light ions.

The release of the new PIXE software in Geant4 is planned in parallel with the completion of the data library and the publication of the model in a refereed journal.

The issue of correct treatment of PIXE in an environment of co-working condensed-random-walk and discrete schemes is foreseen among the topics of a new project concerning core developments of Monte Carlo methods; this project has been submitted to the INFN Technology Scientific Committee and is currently waiting for scientific evaluation and possible funding.

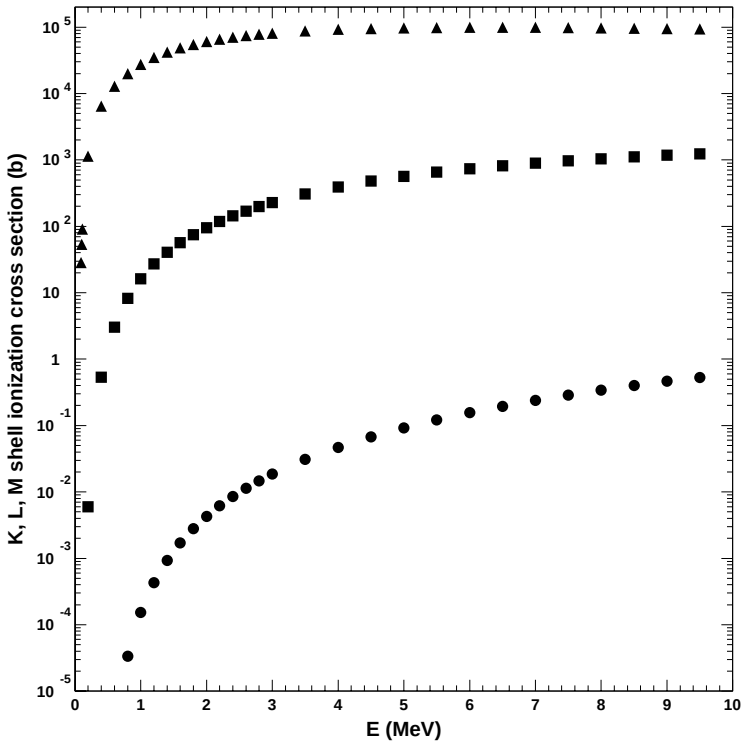

Figure 28 Comparison of Au K (circles), L-total (squares) and M-total (triangles) shell ionization cross sections calculated according to the ECPSSR theoretical model.

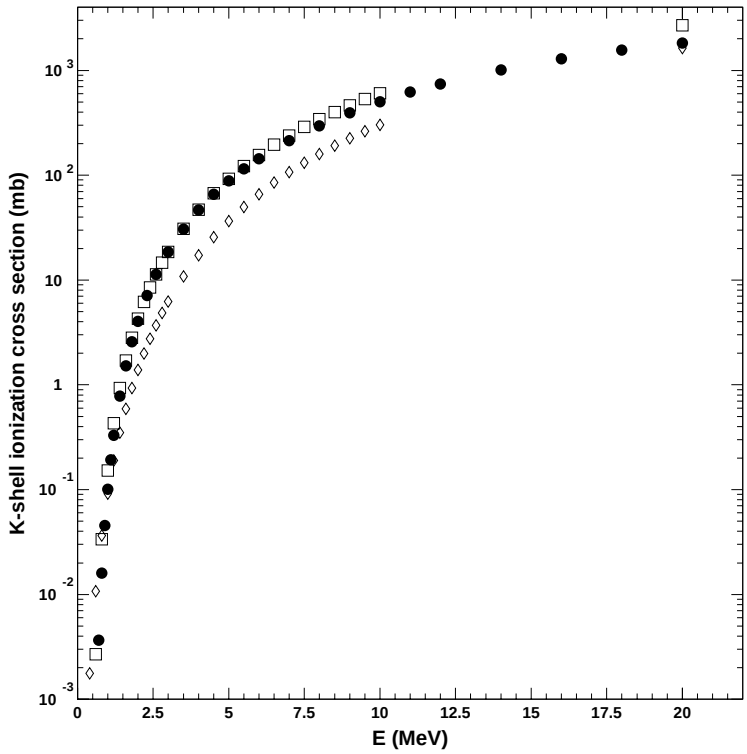

Figure 29 Au K shell ionization cross section: ECPSSR (squares), plane wave Born approximation (diamonds) and experimental data (circles) from [24].

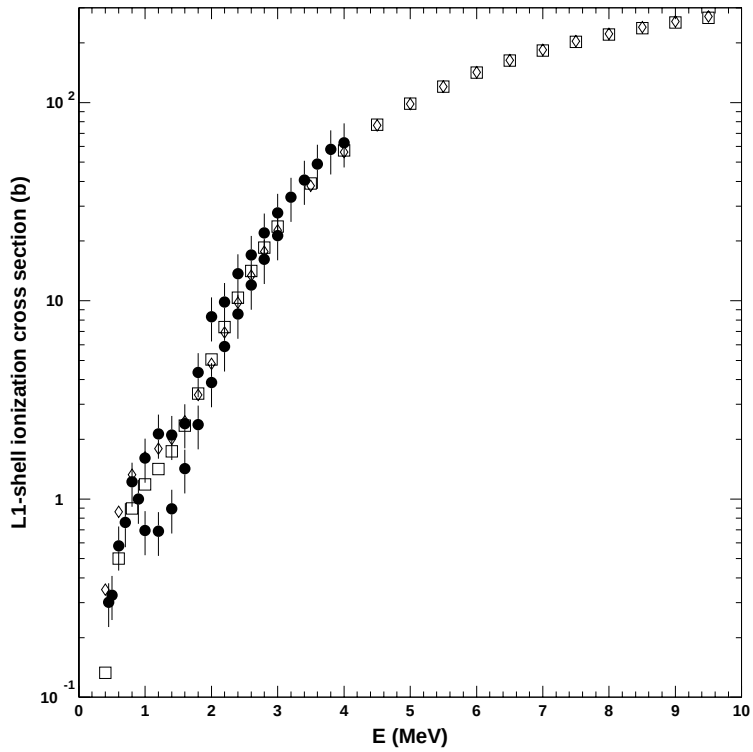

Figure 30 Au L1 shell ionization cross section: ECPSSR (squares), plane wave Born approximation (diamonds) and experimental data (circles) from [29].

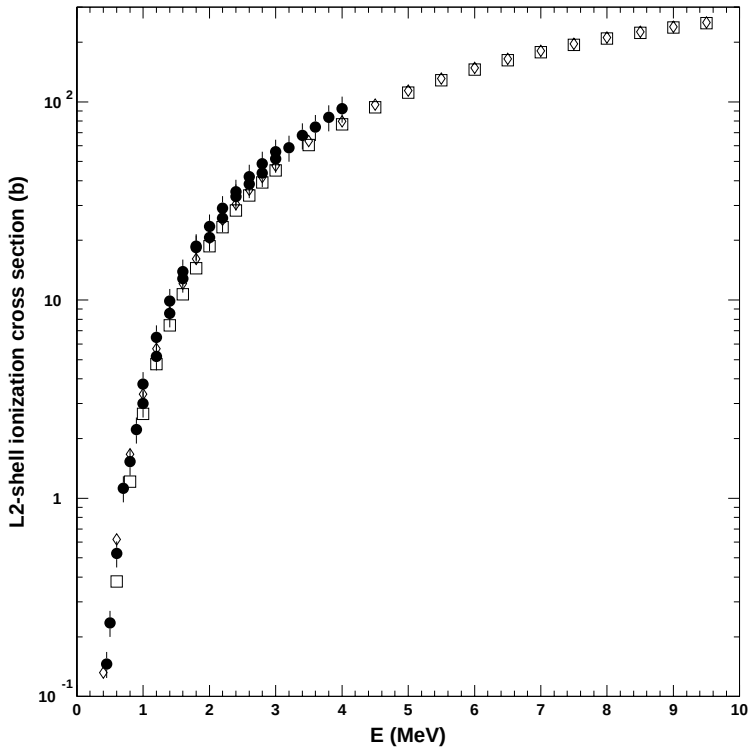

Figure 31 Au L2 shell ionization cross section: ECPSSR (squares), plane wave Born approximation (diamonds) and experimental data (circles) from [29].

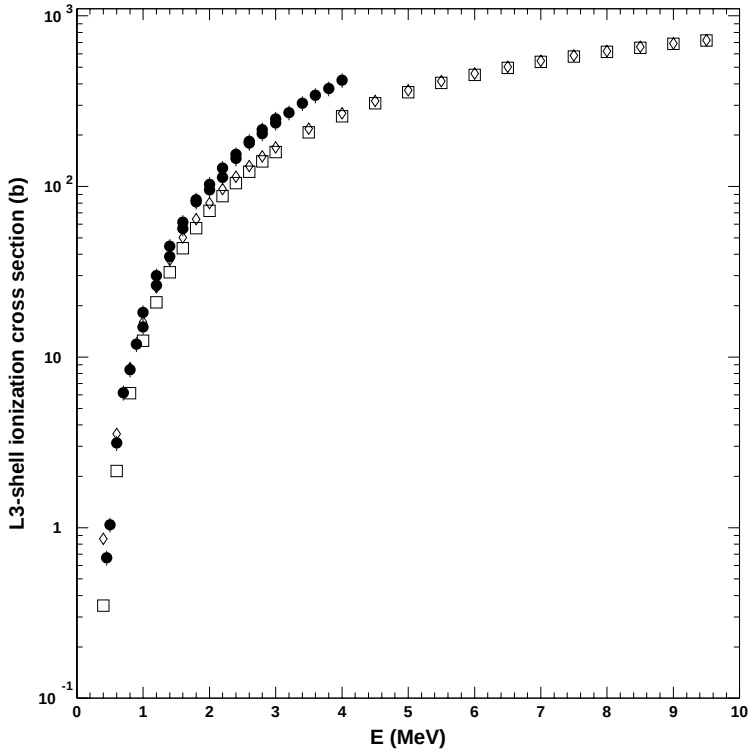

Figure 32 Au L3 shell ionization cross section: ECPSSR (squares), plane wave Born approximation (diamonds) and experimental data (circles) from [29].

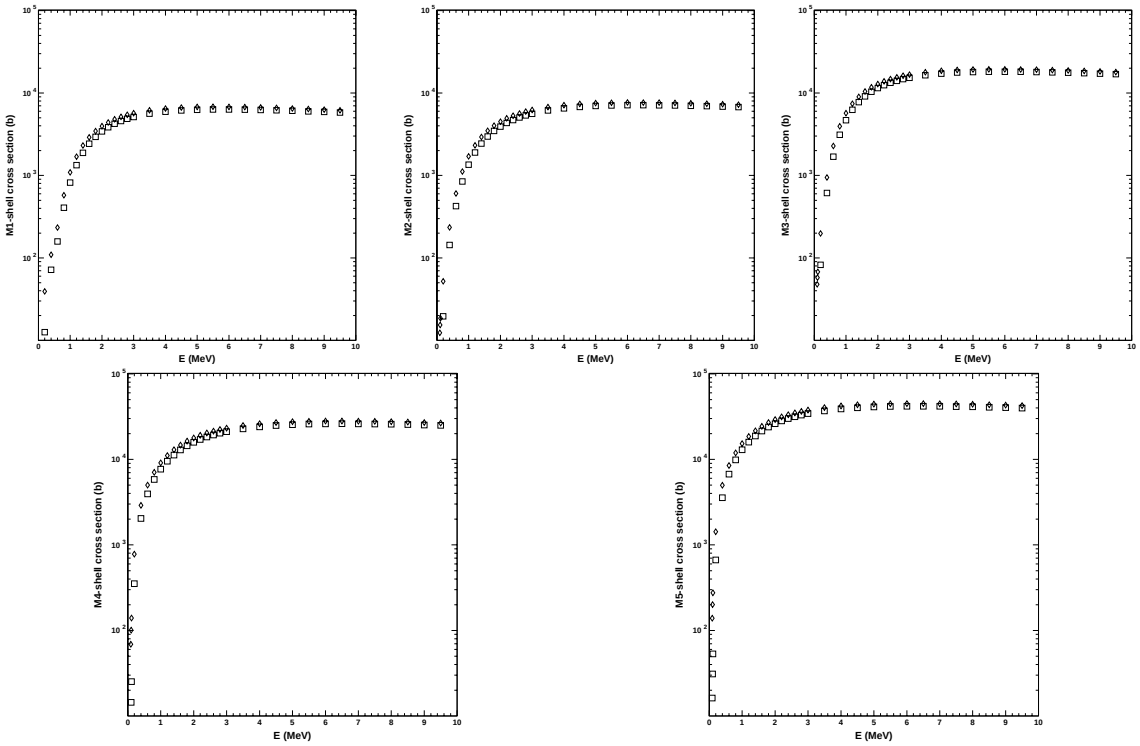

Figure 33 Au M shell ionization cross section: ECPSSR (squares), plane wave Born approximation (diamonds).

4 Conclusion and outlook

The development of Geant4-based anthropomorphic phantom models has provided the scientific community a useful tool for radiation protection studies in various environments, including manned space missions. The original object oriented design conceived in this project enables a variety of configurations with unprecedented flexibility. Further extensions of this project are in progress in collaboration with scientists of the Brazilian Institute of Radioprotection and Dosimetry and the State University of Rio de Janeiro.

The test against the reference data in [13] represents the first systematic validation of Geant4 low energy electromagnetic models concerning the accuracy of the resulting energy deposit; it demonstrated their accuracy against high precision experimental measurements. Since these data have constituted a playground for the evaluation of major Monte Carlo codes, the results strengthen the confidence of Geant4-based simulation in low energy experimental applications. The comparison of different Geant4 versions documented the effect of the evolution of Geant4 multiple scattering algorithm in the low energy domain in a realistic experimental configuration.

The first systematic investigation of PIXE simulation with Geant4 has identified a set of theoretical models to describe the cross sections for the creation of shell vacancies resulting from impact ionization. The theoretical approach is suitable to describe the process for incident protons and heavier ions. The model is capable to handle the creation of vacancies in K, L and M shells. Preliminary evaluations of cross section models have demonstrated the satisfactory accuracy against experimental data; nevertheless, the systematic errors affecting the experimental data are still large. A method to extend the models to higher energies than those concerned in typical material analysis applications has been devised.

The investigation of PIXE modelling has identified serious issues concerning the description of this secondary process in a condensed-random-walk Monte Carlo scheme, as the current treatment of ionization in Geant4 (and in other major Monte Carlo codes). A large-scale project has been submitted to the pertinent INFN scientific committee to address this methodological and architectural issue in the larger context of Monte Carlo kernel R&D.

All the developments and results described in this report are intended to be published in refereed journals. The results described in this report will be presented at the 2008 IEEE Nuclear Science Symposium.

5 Acknowledgement

The work described in this report includes contributions from S. Guatelli, former INFN Genova (section 1), A. Lechner, Technical Univ. of Vienna (section 2), M. Piergentili, Univ. of Genova (section 1), M. Sudhakar, Univ. of Calicut (section 2); it has profited of discussions with M. Begalli, State Univ. Rio de Janeiro and D. de Souza Santos, IRD (section 1), G. Weidenspointner, MPI and A. Zucchiatti, INFN Genova (section 3).

6 Bibliography

[1] H. L. Fisher and W. S. Snyder, "Distribution of dose in the body from a source of gamma rays distributed uniformly in an organ", Proc. IRPA 1, pp. 1473-1486, Rome, 1966.

[2] W. S. Snyder, M. R. Ford M R, G. G. Wamer and H. L. Fisher, "MIRD Pamphlet No. 5 Revised, Estimates of absorbed fractions for monoenergetic photon sources uniformly distributed in various organs of a heterogeneous phantom", J. Nucl. Med. Suppl., no. 3, pp. 5-52, 1969.

[3] M. Cristy and K. F. Eckerman, "Specific absorbed fractions of energy at various ages from internal photon sources", ORNL/TM-8381/V1, Apr. 1987.

[4] E. Y. Han, W. E. Bloch, and K. F. Eckerman, "Revisions to the ORNL series of adult and pediatric computational phantoms for use with the MIRD schema", *Health Phys.*, vol. 90, no. 4, pp. 337-356, 2006.

[5] M. Caon, "Voxel-based computational models of real human anatomy: a review", Rad. Env. Biophys., vol. 42, no. 4, Feb. 2004.

[6] J. Peter, M. P. Tornai and R. J. Jaszczak, "Analytical Versus Voxelized Phantom Representation for Monte Carlo Simulation in Radiological Imaging", *IEEE Trans. Nucl. Sci.*, vol. 19, no. 5, pp. 556-564, 2000.

[7] S. Agostinelli et al., "Geant4 - a simulation toolkit", *NIM A*, vol. 506, no. 3, pp. 250-303, 2004.

[8] J. Allison et al., "Geant4 developments and applications", *IEEE Trans. Nucl. Sci.*, vol. 53, no. 1, pp. 270-278, Feb. 2006.

[9] E. Gamma, R. Helm, R. Johnson, and J. Vlissides, "Design Patterns: Elements of Reusable Object-Oriented Software", Ed.: Addison –Wesley, 1994.

[10] G. Booch, J. Rumbaugh and I. Jacobson, "The Unified Modeling Language User Guide", Addison-Wesley, 1999.

[11] R Chytracek et al., "Geometry Description Markup Language for Physics Simulation and Analysis Applications", *IEEE Trans. Nucl. Sci.*, vol. 53, no. 5, pp. 2892-2896, 2006.

[12] D. R. Dance et al., "Breast dosimetry using high-resolution voxel phantoms", *Rad. Prot. Dosim.*, vol. 114, no. 1-3, pp. 359-363, 2005.

[13] G.J. Lockwood et al., "Calorimetric Measurement of Electron Energy Deposition in Extented Media - Theory vs Experiment", SAND79-0414 UC-34a, 1987.

[14] J. A .Halbleib and T. A. Mehlhorn, "ITS: The Integrated TIGER Series of coupled electron/photon Monte Carlo transport codes", SAND-84-0573, 1984.

[15] J.-F. Carrier, L. Archambault, and L. Beaulieu, "Validation of GEANT4, an object-oriented Monte Carlo toolkit, for simulations in medical physics", *Med. Phys.*, vol. 31, no. 3 , pp. 484-492, 2004.

[16] O. Kadri, V.N. Ivanchenko, F. Gharbi and A. Trabelsi, "GEANT4 simulation of electron energy deposition in extended media", *Nucl. Instr. Meth. B*, vol. 258, no. 2, pp. 381-387, 2007.

[17] K. Amako et al., Comparison of Geant4 electromagnetic physics models against the NIST reference data, *IEEE Trans. Nucl. Sci.*,vol. 52, no. 4, pp. 910-918, Aug. 2005.

[18] J. Apostolakis, S. Giani, M. Maire, P. Nieminen, M.G. Pia, and L. Urban, "Geant4 low energy electromagnetic models for electrons and photons", INFN/AE-99/18, Sep. 1999.

[19] S. Chauvie et al., “Geant4 Low Energy Electromagnetic Physics”, in *Conf. Rec. 2004 IEEE Nucl. Sci. Symp.* Vol. 3, pp. 1881 – 1885, Oct. 2004.
[20] S.T. Perkins et al., Tables and Graphs of Atomic Subshell and Relaxation Data Derived from the LLNL Evaluated Atomic Data Library (EADL), Z=1-100, UCRL-50400 Vol. 30, 1997.
[21] S.T. Perkins et al., “Tables and Graphs of Electron-Interaction Cross Sections from 10 eV to 100 GeV Derived from the LLNL Evaluated Electron Data Library (EEDL)”, UCRL-50400 vol. 31, 1997.
[22] D. Cullen et al., EPDL97, the Evaluated Photon Data Library, UCRL–50400, Vol. 6, Rev. 5, 1997.
[23] J. Sempau, J. M. Fernández-Varea, E. Acosta, and F. Salvat, “Experimental benchmarks of the Monte Carlo code PENELOPE”, *NIM B,* vol. 207, no. 2 , pp. 107-123, Jun. 2003.
[24] H. Paul and O. Bolik, “Fitted empirical Reference Cross Sections for K-Shell Ionization by Alpha Particles”, *At. Data Nucl. Data Tables,* vol. 54, pp. 75-131, 1993.
[25] S. Guatelli, A. Mantero, B. Mascialino, P. Nieminen, and M. G. Pia, “Geant4 Atomic Relaxation”, *IEEE Trans. Nucl. Sci.*, vol. 54, no. 3, pp. 585-593, Jun. 2007.
[26] W. Brandt and G. Lapicki, “Energy-loss effect in inner-shell Coulomb ionization by heavy charged particles”, *Phys. Rev. A*, vol. 23, pp. 1717 – 1729, 1981.
[27] G. Lapicki, “The status of theoretical K-shell ionization cross sections by protons”, X-Ray Spectrometry, vol. 34, no. 4, pp. 269 – 278, 2004.
[28] E. Merzbacher and H. Lewis, “Encyclopedia of Physics”, vol. 34, p. 166, Springer,Verlag, Berlin (1958).
[29] I. Orlic, C.H Sow and S.M. Tang, “Experimental L-shell x-ray production and ionization cross sections for proton impact”, *At. Data Nucl. Data Tables*, vol. 56, pp. 159-210, 1994.